

## Microstructure Measurements from a Towed Undulating Platform

MICHAEL W. OTT, JOHN A. BARTH, AND ANATOLI Y. EROFEEV

*College of Oceanic and Atmospheric Sciences, Oregon State University, Corvallis, Oregon*

(Manuscript received 26 June 2003, in final form 9 February 2004)

### ABSTRACT

MicroSoar, an undulating profiler capable of measuring turbulence parameters such as Thorpe scales and thermal dissipation rate while being towed at speeds of up to  $4 \text{ m s}^{-1}$ , offers the possibility of obtaining a close-to-synoptic image of mixing over large spatial areas. In this paper, the method of calculating Thorpe scales from the high-frequency MicroSoar data is developed, and results from data taken off the coast of Oregon during the summer of 2001 are presented. Large Thorpe scales and elevated measurements of the thermal dissipation rate are shown to be associated with shear at the edge of the coastal jet. It is further shown that using MicroSoar data rather than Sea-Bird conductivity–temperature–depth data extends the range of measurable overturns to smaller scales, particularly in regions of low stratification.

### 1. Introduction

Away from solid boundaries and the interfaces of water masses, molecular frictional forces are weak compared to Coriolis and pressure forces. That much of the ocean's currents are in geostrophic balance provides confirmation that “the direct effect [of friction] on large-scale motion has been shown . . . to be utterly negligible” (Pedlosky 1979). Nevertheless, the fact that both oceanic currents and external forcing (such as solar radiation and wind stress) are steady in time, when averaged appropriately, indicates that friction is vital in removing energy from large-scale flows. Although global currents are too large in scale for molecular friction to work against directly, the length scales in any geophysical flow cover the spectrum from that of the main flow to the scales small enough that molecular diffusion is important. In an average sense, energy is continuously removed from shear in large-scale flows, cascaded through turbulent eddies of ever decreasing size, and eventually dissipated into heat energy at molecular scales.

Recognizing both that frictional effects need to be considered in the dynamics of oceanic flows and that the range of length scales involved is too large to allow for resolution of the small-scale turbulent eddies themselves, there is clearly a need to parameterize these viscous effects. That is, the dissipation of energy (at small scales) taken from the large-scale flow must be related to properties of the main flow only.

Before this can be done, however, a better understanding of turbulence itself is required. A major impediment to this goal is the relative lack of turbulence measurements, particularly in the coastal ocean, where Gargett (1994) argues that “dissipative structures can be undersampled” because “turbulent flows . . . are energetic and vary rapidly in both time and space.” Therefore, large volumes must be sampled in order to obtain meaningful averages of turbulent mixing. Currently popular loosely tethered free-falling microstructure profilers (Moum et al. 1995; Caldwell et al. 1985; Newberger et al. 1984) are a vast enhancement over the previous generation of instruments that recorded internally, used ballast weights, and had to be recovered after each profile (see discussion in Gregg 1998).

The recently developed MicroSoar (May 1997; Dillon et al. 2003), a microstructure sampling system attached to the towed undulating SeaSoar (Pollard 1986) platform, can sample over a length a magnitude of order larger than tethered profilers. While direct measurements of turbulence using shear probes are not possible with MicroSoar, owing to typical tow speeds of  $3.5 \text{ m s}^{-1}$ , estimates of the turbulent dissipation rate  $\epsilon$  can be made by first calculating Thorpe scales. MicroSoar does measure the temperature variance dissipation rate  $\chi$  directly, however (Dillon et al. 2003).

Thorpe scales (Thorpe 1977; Dillon 1982)  $L_T$  are a measure of the length scale of turbulent events, which can be calculated from the density data. Dissipation rates can then be calculated by determining the work that each of these overturns did against the background stratification (Galbraith and Kelley 1996). Recently, Ullman et al. (2003) used density measurements from a Sea-Bird 911+ conductivity–temperature–depth (CTD) in-

---

*Corresponding author address:* Dr. Michael W. Ott, College of Oceanic and Atmospheric Sciences, 104 Ocean Admin. Building, Oregon State University, Corvallis, OR 97331-5503.  
E-mail: mwott@coas.oregonstate.edu

strument mounted on SeaSoar taken off Georges Bank to calculate Thorpe scales. They found that  $L_T$  was undersampled in comparison to free-falling microstructure instruments, although they did not have any coincident microstructure data with which to compare. This was partly due to the fact that while the Sea-Bird 911+ CTD samples both temperature and conductivity at 24 Hz, the frequency response of these instruments is considerably lower. At speeds of  $1 \text{ m s}^{-1}$  (typical SeaSoar vertical velocities at middepth), Gregg and Hess (1985) found that the temperature and conductivity frequency responses (defined as the inverse of the time required for the instrument to reach 63% of the final value following a step change in temperature or conductivity) were closer to 2.5 and 4–10 Hz (depending on flushing rates), respectively.

In this paper, we extend the Thorpe-scale analysis to MicroSoar data, the frequency response of which better matches that of traditional microstructure instruments. As part of the Coastal Ocean Advances in Shelf Transport (COAST) program (Barth et al. 2002), the aim of which is to study cross-shelf wind-driven transport processes, MicroSoar collected approximately 3000 and 4000 undulations in June and August of 2001, respectively, of 2048-Hz conductivity and 256-Hz temperature data. Vertical profiles of microstructure from Chameleon, a free-falling instrument, were also collected from a second vessel (Perlin et al. 2004, manuscript submitted to *J. Geophys. Res.*) operating in the same region at the same time, allowing a comparison with MicroSoar data.

In section 2, the background physical and oceanographic conditions as well as the dataset are described. In the next section, we develop the method for calculating Thorpe scales from the MicroSoar data. In section 4, we compare the resulting overturn lengths, as well as other calculated turbulence parameters, such as the temperature variance dissipation rate, to both the corresponding values calculated from Chameleon data and background parameters such as the gradient Richardson number ( $Ri$ ). In the summary, section 5, these results are related to some of the hypotheses of the COAST project, including mapping the overall microstructure in relation to both the mesoscale hydrographic and flow fields and the bottom topographic features. Some implications for future turbulence work are also examined.

## 2. Data

Two physical oceanography cruises on the R/V *Wecoma* were conducted in the late spring and summer of 2001 as part of the COAST project. The objective of these surveys was to obtain “rapid, high-resolution maps of the three-dimensional thermohaline, bio-optical, zooplankton and velocity fields” (Barth et al. 2002) to complement high-vertical-resolution profiles from Chameleon taken aboard the R/V *Thomas G. Thompson*, surface current maps from land-based coastal radar, and atmospheric measurements from an aircraft. The first of

these cruises, from 23 May to 13 June, occurred early in the upwelling season, while the second, from 6 to 26 August, took place when upwelling was more established. During each cruise, surveys were made off both northern Oregon, where the alongshore topography is rather uniform and the upwelling region is narrow, and off central Oregon, where the continental shelf is much broader and the topography is considerably more three-dimensional (Fig. 1). The data presented here are restricted to transects from the broad continental shelf off the central coast during the May–June cruise.

SeaSoar, an undulating platform equipped with a suite of instruments measuring physical and biooptical properties, was towed behind the R/V *Wecoma* at a speed of approximately  $3.5 \text{ m s}^{-1}$  and sampled the water column from the surface to within 10 m of the bottom to a maximum depth of about 110 m. Among these instruments was a standard Sea-Bird 911+ CTD equipped with dual temperature and conductivity sensors. Sea-Bird claims that its temperature sensors have an accuracy of  $10^{-3}^\circ\text{C}$ , a resolution of  $2 \times 10^{-4}^\circ\text{C}$  at 24 Hz, and a time response of  $6.5 \times 10^{-2} \text{ s}$ , where the latter is defined as the time to reach 63% of the final value following a step change in temperature with a water velocity of  $1 \text{ m s}^{-1}$ ; corresponding parameters for the conductivity probe are  $3 \times 10^{-4} \text{ S m}^{-1}$ ,  $4 \times 10^{-5} \text{ S m}^{-1}$ , and  $6.5 \times 10^{-2} \text{ s}$ . These response times imply a frequency response of approximately 15 Hz. While this is a significant improvement over the previously quoted values Gregg and Hess (1985) determined for earlier probes, it is still considerably less than the 24-Hz rate used in Thorpe-scale calculations.

MicroSoar’s temperature probe is a Thermometric series FP07 glass-coated bead thermistor built at Oregon State University (Dillon et al. 2003) and has a resolution of  $3 \times 10^{-4}^\circ\text{C}$  and a time response of  $5 \times 10^{-2} \text{ s}$ . The conductivity probe is a capillary microconductivity sensor (CMCS) (Paka et al. 1999) with a resolution of  $2 \times 10^{-4} \text{ S m}^{-1}$  and a time response of  $5 \times 10^{-4} \text{ s}$ . A three-axis accelerometer monitors vibrations of the MicroSoar platform. Dillon et al. (2003) discuss the technique for calculating  $\chi$ , the thermal dissipation rate, from microstructure conductivity measurements and demonstrate that towing-induced vibrations do not significantly affect the measurement of microstructure scalars.

A hull-mounted 153-kHz narrowband RD Instruments acoustic Doppler current profiler (ADCP) measured currents almost continuously over the entire cruise (Pierce and Barth 2002), enabling microstructure measurements to be placed in the context of velocity shears associated with jets and the bottom boundary layer. The ADCP was configured with vertical bins of 8-m length and with an ensemble averaging interval of 2.5 min, implying uncertainties in the currents of  $0.013 \text{ m s}^{-1}$ . When calculating Richardson numbers, a smoothed stratification ( $N^2$ ) is used to ensure that the measurement scales are similar to those of the shear: the sorted den-

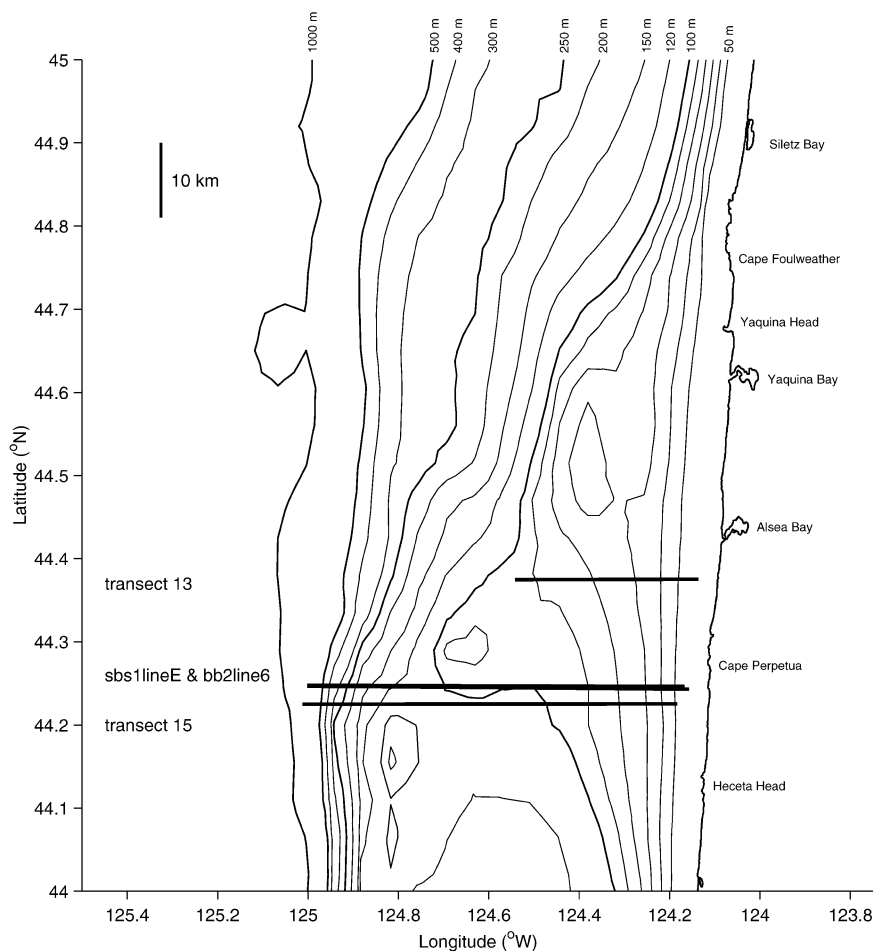


FIG. 1. Bathymetry off the coast of Oregon (m) with selected transects (horizontal bars).

sity, calculated using the Sea-Bird CTD data, is averaged using triangular windows of half-width 2 min and 8 m in the horizontal and vertical directions, respectively. The SeaSoar (stratification) and ADCP (shear) data are aligned temporally and spatially via the GPS time and depth recorded by each instrument.

On several occasions during the first cruise, the *We-coma* made transects in the same area as the *Thompson* (i.e., east–west sections of at least 10 km in length to allow enough profiles for comparison) within 12 h of each other, a short enough time that it may be reasonable to assume that the mixing environments were similar. Unfortunately, during some of these events, including two that featured strong downwelling-favorable winds, MicroSoar was not working properly because of internal ground faults. The two sections used for comparison occurred off central Oregon in a region of complex offshore topography (Fig. 1): one after a relatively weak downwelling-favorable wind event and one after a stronger upwelling-favorable wind event (Fig. 2). We will use these instances to compare microstructure measurements between MicroSoar and Chameleon to demonstrate that MicroSoar can be a valuable addition to the

turbulence community. First, we turn to the technique used to determine Thorpe scales from the combined Sea-Bird 911+ CTD and MicroSoar data.

### 3. Method

The Sea-Bird CTD system aboard SeaSoar employs pumped dual temperature and conductivity sensors sampling at 24 Hz. The sensors are mounted pointing forward in a hole in the nose of SeaSoar (Fig. 3). Pumping, along with sensor design to match response times, helps reduce errors in the derived salinity signal. Software is used to correct the remaining response mismatch error, which is partly due to variable flow rates past the sensors as SeaSoar dives. The thermal mass of the conductivity cell is corrected for by following the method of Lueck (1990). For further details, see Barth et al. (2000). The temperature and conductivity sensors were calibrated by Sea-Bird on 29 and 30 March 2001, respectively.

The Sea-Bird CTD sensors are designed to have minimal drift over time; this stability is achieved at the expense of instrument sensitivity. The MicroSoar sensors, on the other hand, are very sensitive but more

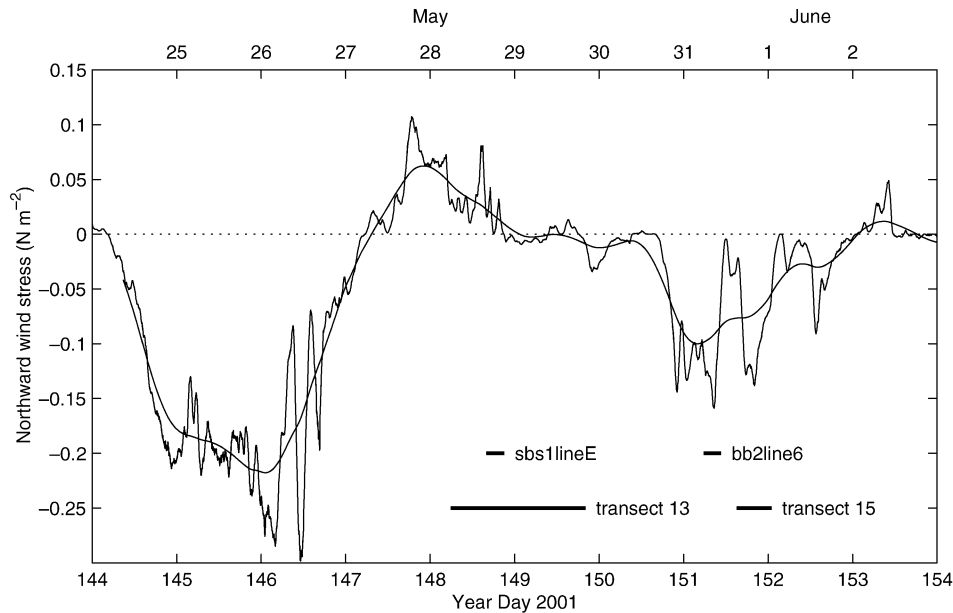


FIG. 2. Northward wind stress ( $\text{N m}^{-2}$ ) during the COAST experiment (thin line), with 24-h running mean (thick line) and times of selected transects (horizontal bars).

susceptible to drift. The sensors are mounted at the front of the MicroSoar package underneath SeaSoar (Fig. 3). After averaging both the Sea-Bird and MicroSoar data to 1 Hz, the MicroSoar temperature, conductivity, and pressure data are calibrated by linear regression against the Sea-Bird data in 5-min sections. The regression coefficients show very little drift over time (Dillon et al. 2003) and have only a few outliers, which are generally due to problems with the MicroSoar analog electronics.

It is not possible to resolve overturns at scales smaller than the Batchelor scale,  $\kappa_B$ , since molecular diffusion removes variance faster than it is produced by the strain rate. In the ocean,  $\kappa_B \approx 0.01$  m, and with vertical speeds of the SeaSoar platform exceeding  $0.25 \text{ m s}^{-1}$  through-

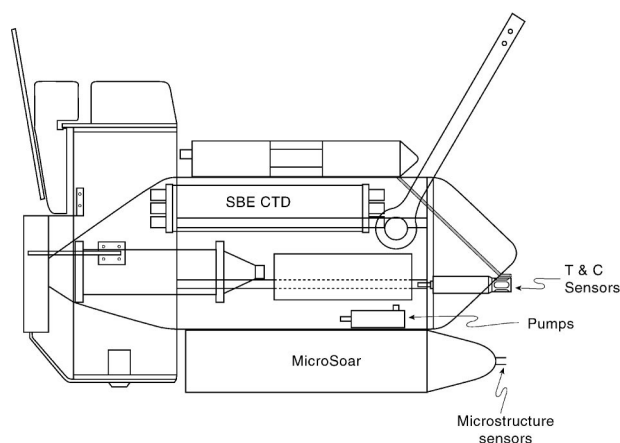


FIG. 3. Schematic of SeaSoar as equipped for use during the COAST experiment.

out most of the water column in each undulation, examining the MicroSoar data at frequencies above 25 Hz does not yield additional information. The MicroSoar pressure, temperature, and conductivity data are thus filtered using an elliptic filter of order 8 and frequency cutoff of 25.6 Hz and is then block-averaged to 25.6 Hz.

Many of the steps used to calculate Thorpe scales from the MicroSoar data are those Ullman et al. (2003), following Galbraith and Kelley (1996), employed for 24-Hz Sea-Bird data from the SeaSoar. For example, to limit the extent to which horizontal density variations affect calculated overturns and to prevent biases against large overturn sizes, only sections in which the vertical speed exceeds  $1.0 \text{ m s}^{-1}$  (i.e., for which the attack slope is at least 0.3) and which are at least 20 m in vertical length are used. The minimum vertical speed was increased from  $0.25 \text{ m s}^{-1}$ , the value Ullman et al. (2003) used, in light of the fact that nonlinear solitons with slopes approaching 0.3 can occur off the Oregon shelf in the presence of shear (Moum et al. 2003). Thorpe (1978) found that the maximum internal wave slope that can exist in flows without shear is 0.34; in the presence of even modest shear, the maximum stable slopes fall below 0.3.

For upward casts, the former criterion often results in the loss of a considerable portion of the top of the profile, with minimal loss at the bottom; for downward casts, the loss at the top is typically several meters, while that at the bottom is generally quite substantial. For the 24-Hz Sea-Bird data, the calculated density is then sorted to calculate potential overturns in the standard way (Thorpe 1977). Real overturns are identified as those

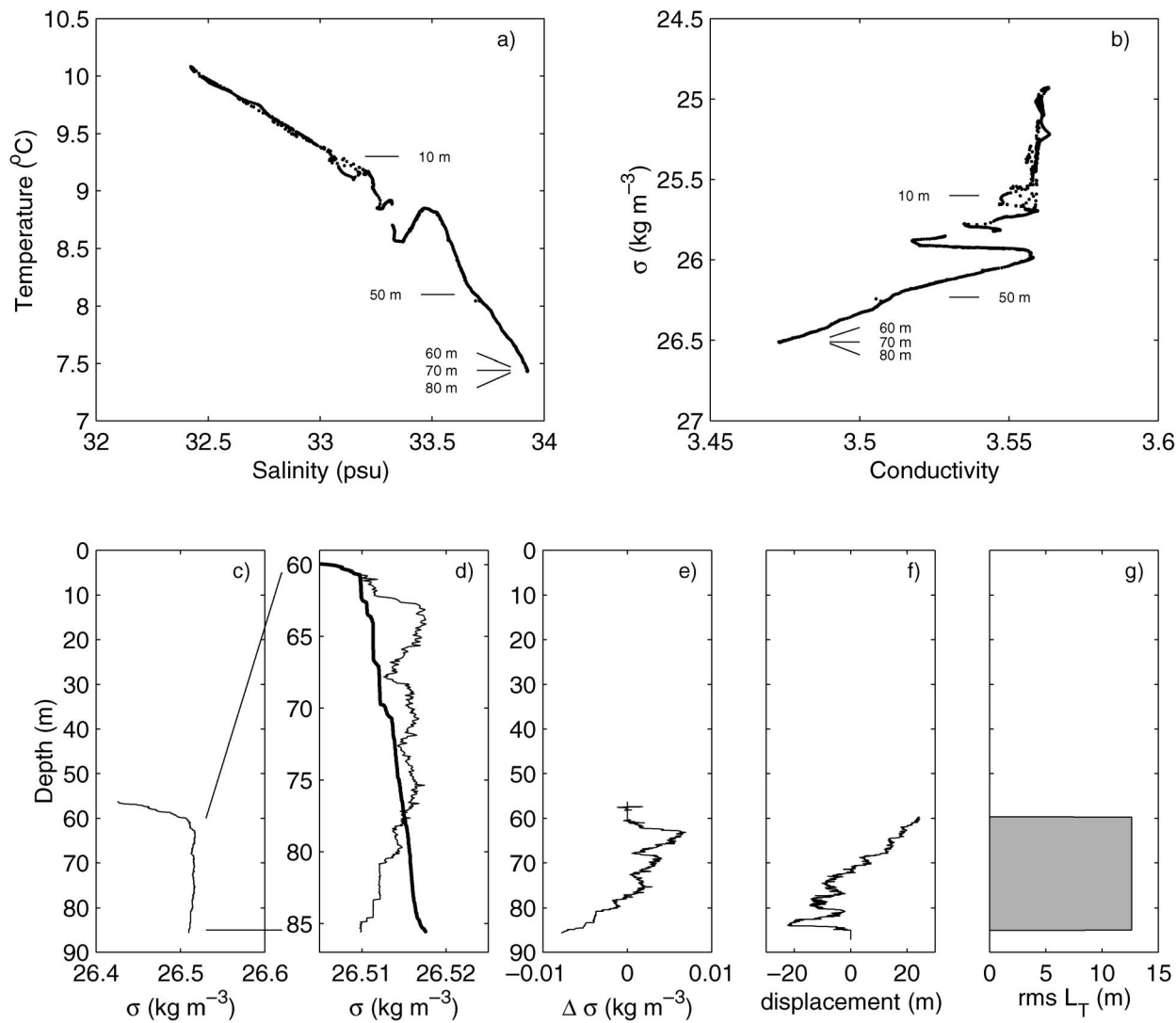


FIG. 4. Method for calculating Thorpe scales as applied to an individual MicroSoar cast from transect bb2line6: (a) temperature–salinity plot and (b) conductivity–density based on 24-Hz Sea-Bird CTD data, (c) MicroSoar density from MicroSoar conductivity [gaps indicate regions where relationship in (b) is nonlinear], (d) detail of individual reordering region with measured (thin) and sorted (thick) density, (e) Thorpe fluctuation, (f) corresponding Thorpe displacement for those reordering regions that meet criteria, and (g) associated root-mean-square Thorpe scale.

that pass a number of criteria proposed by Galbraith and Kelley (1996), including resolution tests for both the thickness and density differences and a water-mass test to exclude inversions arising from mismatches in the time response of the temperature and conductivity probes.

Whereas the Sea-Bird CTD system utilizes a flow-through system, ensuring that the temperature and conductivity probes sample the same volume of water, the same is not true for MicroSoar, of which the T and C probes are fixed 0.10 m apart on the underside of the SeaSoar platform (Fig. 3). The density calculated using the MicroSoar temperature and conductivity probes together is thus not a reliable estimate of the true density; the T–S diagram is much less linear than that for the

corresponding Sea-Bird 24-Hz data. It is not surprising, therefore, that the vast majority of potential overturns calculated using the MicroSoar density fail the water-mass test.

To calculate Thorpe scales from MicroSoar data requires that the density be determined from only one of the probes, and since the FP07 thermistor has a lower-frequency response (−3 dB at 20 Hz), the conductivity probe is used. In order to do this, the densities calculated from the Sea-Bird temperature and salinity data (Fig. 4a) are linearly regressed on the Sea-Bird conductivity data to create a lookup table (Fig. 4b). A similar procedure was employed by Crawford (1986), whose vertical turbulence profiler measured only temperature. Crawford calculated density using temperature and sa-

linity from CTD casts taken within an hour of the turbulence profiles, whereas we have the advantage of measuring density from the nearly collocated Sea-Bird CTD sensors. Best-fit lines for depth ranges of at least 1 m and containing at least 10 data points are calculated, with the slope and intercept then used to obtain density from the MicroSoar conductivity data over those same depth ranges (Fig. 4c). It is not possible, therefore, to calculate overturns based on the MicroSoar data in regions for which the Sea-Bird conductivity–density relation is not piecewise linear. As a result, high-resolution density data are not available for about 10% of the water column for a typical profile, a loss which is approximately equal to the number of potential overturns calculated from the Sea-Bird data that fail the water-mass test.

Overturns are then calculated from this MicroSoar density in the same manner as for the Sea-Bird data. Potential overturns (Fig. 4d) are identified within reordering regions (Galbraith and Kelley 1996), or “complete overturns” (Dillon 1984), by examining the difference between the measured and sorted density profile. This Thorpe fluctuation (Fig. 4e) corresponds to a Thorpe displacement (Fig. 4f), distances water parcels in the background (i.e., sorted, stable) density profile moved as a result of overturning eddies, which can be of either sign. To obtain Thorpe scales, these displacements are averaged vertically in a root-mean-square sense. This is generally done over scales representative of the overturns themselves, although what this scale should be is less than obvious. Following Ullman et al. (2003), the averaging is done over the entire length of the reordering region (Fig. 4g).

To facilitate comparison of the resulting Thorpe displacements to those calculated from traditional free-falling microstructure instruments, density data from the Chameleon is processed in the same manner. While it is unreasonable to expect similarities between individual profiles given the intermittent nature of turbulence, statistical representations, such as probability density functions of overturn size, should be comparable for similar mixing regimes.

## 4. Results

### a. *MicroSoar*

An east–west transect at 44.24°N obtained on 28 May 2001, sbs11lineE, reveals the classic shoaling of isopycnals toward the coast in response to upwelling-favorable winds (Fig. 5a). The associated southwestward coastal jet, above Heceta Bank, is confined to the upper part of the water column and isolated from the coast by an area of recirculation to the north (Fig. 5f). In the region between the jet and recirculation, there is some divergence in  $U$ , the zonal flow (Fig. 5e). The large Thorpe signal (Fig. 5c) seen in the MicroSoar data just above and inshore of Heceta Bank is confined to depths below

60 m due to fairly strong stratification (Fig. 5b) at the edge of the jet, even though the shear (Fig. 5g) is large. This region of strong eddy activity matches very well that where the very weak stratification causes the Richardson number to fall below 0.1 (Fig. 5h).

The strong overturn signal near Heceta Bank (Fig. 5c) is seen in only every second cast (the upward casts); on downward casts, the SeaSoar trace levels out as the bottom of each cast is approached, resulting in vertical instrument speeds of less than 1.0 m s<sup>-1</sup>. In addition, because the instrument is not flown closer than 10 m to the bottom, particularly in regions where the topography changes abruptly, it is not known how much deeper, or indeed how much farther west to the bank, this region of large overturns extends. Thus, although it appears that the Thorpe signal is a result of Heceta Bank, it is not possible to show this conclusively. This loss of data, compared to free-falling instruments, for example, is the trade-off for the ability to sample quickly over large areas.

Weaker and more intermittent Thorpe signals, which may be related to the sloping bottom, are seen at about 124.3°W and 50-m depth, where the stratification is also weak. The overturns are seen in both the up- and downward casts, extending up to depths of 30 m within the recirculation zone. Unfortunately, the absence of shear measurements makes the calculation of Richardson numbers impossible in this region. There are large  $\chi$  values at 124.9°W and 70-m depth, at the upper edge of a deeper poleward jet, where low Richardson numbers are due to strong shear instead of reduced stratification. This signature of small-scale mixing is accompanied by a few elevated Thorpe-scale measurements, though the signal is not overwhelming. Similarly, there is a suggestion of overturns at 124.8°W and 20-m depth, which may lie beneath an oceanward extension of the southward coastal jet.

The relationship between stability and overturn size is better seen in scatterplots (Fig. 6), although the nature of associating large-scale parameters to mixing parameters means that these correlations are not always easy to visualize. For example, while density, Thorpe displacements, and thermal dissipation are measured at scales of centimeters vertically, the ADCP current is measured in 8-m bins vertically. In order to more closely match the spatial scales, the density data are smoothed vertically, with a triangular filter of half-width equal to that of the ADCP bin size (8 m), and horizontally before the buoyancy frequency is calculated, as was done for the Richardson number calculations in Fig. 5. While large overturns are clearly associated with weaker stratification (Fig. 6a), there is no apparent relationship between overturn size and shear (Fig. 6b), although the large overturns are found to the right of the midpoint of the shear ( $7 \times 10^{-6} \text{ s}^{-2}$ ). The largest overturns have mean Richardson numbers below unity (Fig. 6c), with the majority at or below the 0.25 linear stability criterion.

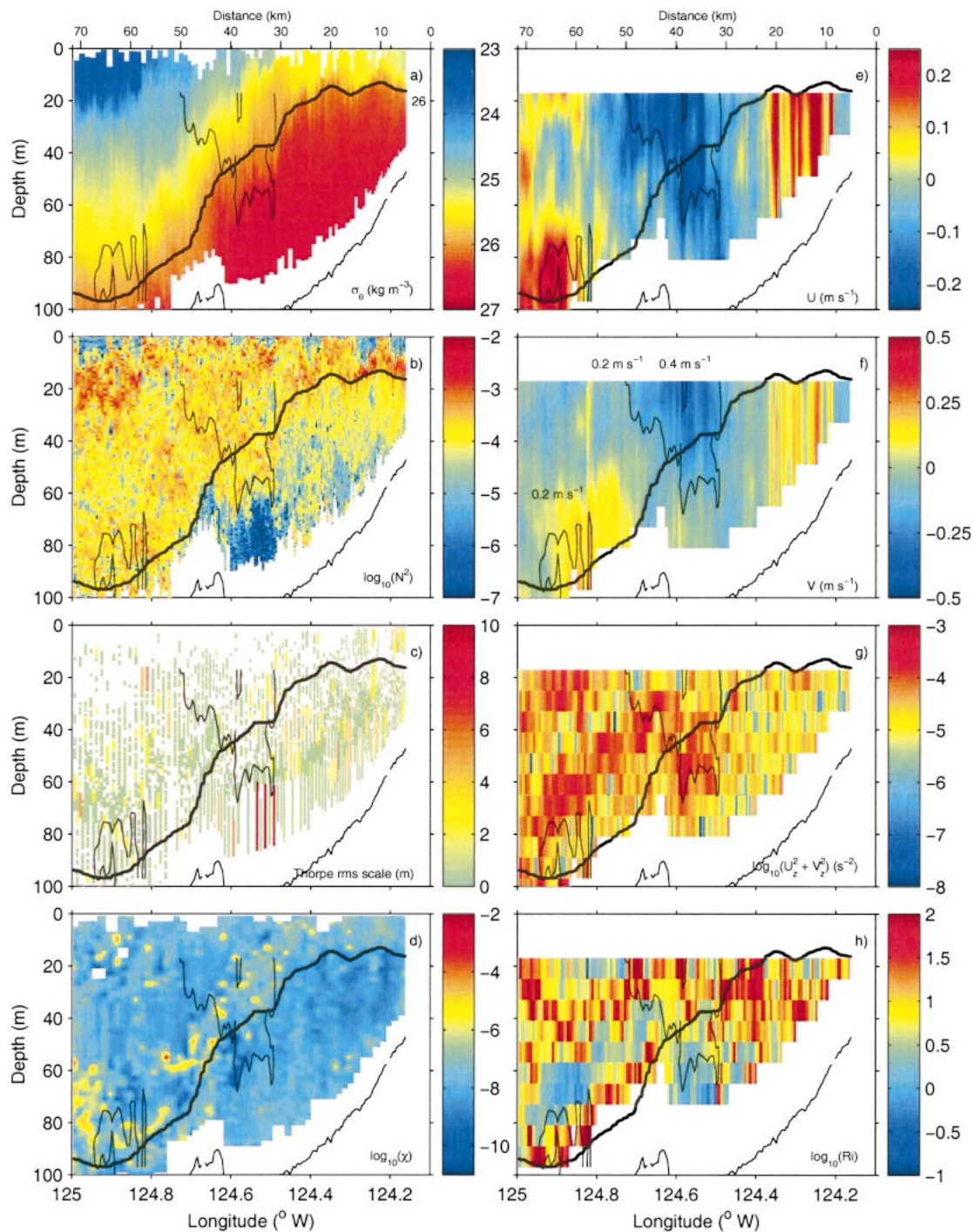


FIG. 5. Flow properties for transect sbs1lineE: (a)  $\sigma_\rho$  ( $\text{kg m}^{-3}$ ), (b) buoyancy frequency squared ( $\text{s}^{-2}$ ), (c) calculated rms Thorpe scale (m), (d) thermal dissipation rate ( $^\circ\text{C}^2 \text{s}^{-1}$ ), (e) east–west velocity ( $\text{m s}^{-1}$ ), (f) north–south velocity ( $\text{m s}^{-1}$ ), (g) shear squared ( $\text{s}^{-2}$ ), and (h) Richardson number. The  $1026 \text{ kg m}^{-3}$  isopycnal is denoted by the thick line, while the thin lines are the  $0.2$  and  $0.4 \text{ m s}^{-1}$  contours of the total speed.

On the other hand, while the largest thermal dissipation rate measurements are associated with the strongest shear (Fig. 6e), they are associated with stronger stratification (Fig. 6d). As a result, there is no clear

relationship between large thermal dissipation rates and Ri (Fig. 6f), though one would perhaps not expect a strong relationship since thermal energy dissipates at scales considerably smaller than the buoyancy scale,  $L_b$ ,

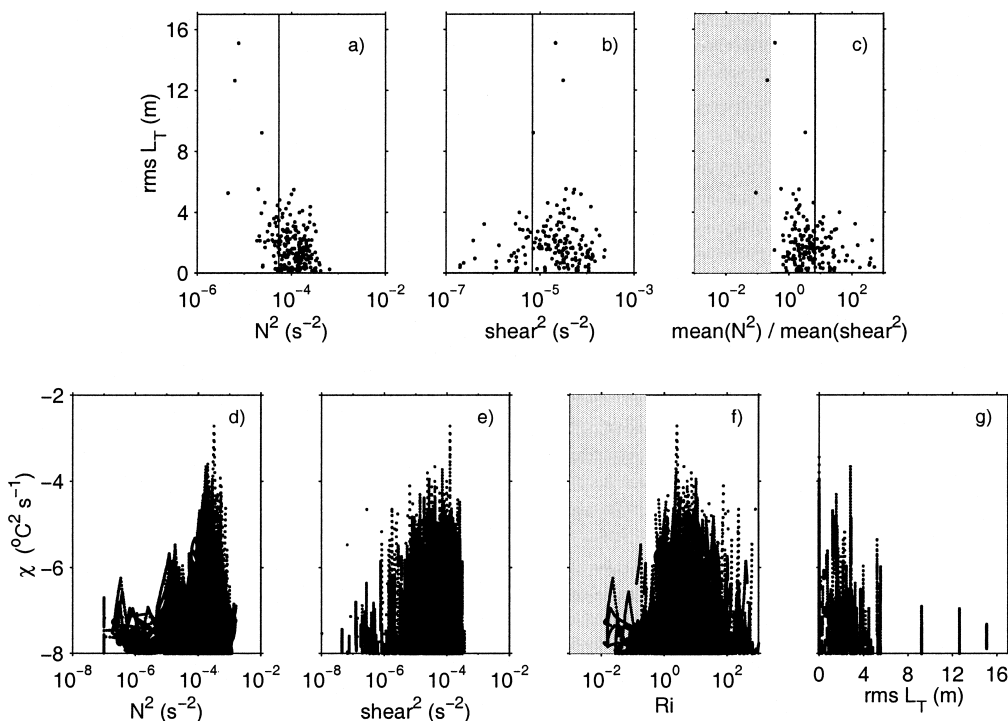


FIG. 6. Relationship between flow and mixing parameters for transect sbs1lineE. In (a)–(c) each point represents the rms Thorpe displacement (m) over an overturning region, and the solid line indicates the median independent variable. In (d)–(g) each point represents a single measurement of the thermal dissipation rate ( $^{\circ}\text{C}^2 \text{s}^{-1}$ ). Values below  $10^{-8}$  are within the noise band and are not shown. In (c) and (f) the shaded region represents  $\text{Ri} < 0.25$ .

$= 2\pi (\epsilon/N^3)^{1/2}$ , the length scale of the largest eddies that can be sustained without being impeded by stratification.

Finally, there is no clear relation between overturn scales and thermal dissipation rates themselves (Fig. 6g). In the image of sbs1lineE (Fig. 5d), low values of thermal dissipation are seen just above and inshore of Heceta Bank, where the largest Thorpe displacements are seen. This is perhaps not surprising, since overturns and dissipation are different stages in the cascade of energy from large-scale flow to thermal energy, with dissipation occurring only after large eddies have become much smaller. During this time, not only do conditions following the flow change, but the background current transports different water masses into the area. The larger thermal dissipation values at 60-m depth directly above Heceta Bank, for example, may be the result of overturns that occurred at that location earlier, but it is also possible that overturns generated earlier just inshore of Heceta Bank (in the same region that they are seen in Fig. 5) were transported oceanward and upward by the diverging zonal flow.

A transect at the same location about 60 h later, bb2line6 (Fig. 7), reveals a coastal jet that is considerably stronger and larger in cross-sectional area (Figs. 7e and 7f). At the same time, zonal flows are noticeably weaker; that is, the coastal jet is aligned in a more north–

south direction. Nevertheless, although the magnitude of the largest Thorpe scales (Fig. 7c) is somewhat smaller than for transect sbs1lineE (Fig. 5c), the distribution is remarkably similar: increased eddy activity is seen at 60 m west of the jet ( $124.8^{\circ}\text{W}$ ), at 20 m above the sloping bottom between  $124.3^{\circ}$  and  $124.2^{\circ}\text{W}$ , and just beneath the southward coastal jet (above and inshore of Heceta Bank).

In the latter case, SeaSoar was not flown as close to the bottom during the bb2line6 transect (cf. sbs1lineE), so fewer overturns are seen. Compared to transect sbs1lineE, where low Richardson numbers (Fig. 5h) just above and inshore of Heceta Bank resulted from weak stratification (Fig. 5b) overcoming weak shear (Fig. 5g), the low Ri values for transect bb2line6 (Fig. 7h) result from strong shear (Fig. 7g); stratification is considerably stronger (Fig. 7b). This suggests that, for bb2line6 at least, mixing is associated with the edge of the jet and not with topography. This may also be the case for the corresponding region of transect sbs1lineE (Figs. 5c and 5h), as the horizontal separation from Heceta Bank is several kilometers and mixing levels directly above the bank are relatively weak. Unfortunately, without measurements to isolate the overturning region from the bottom, as for bb2line6, firm conclusions cannot be drawn.

The weakest stratification seen in transect bb2line6

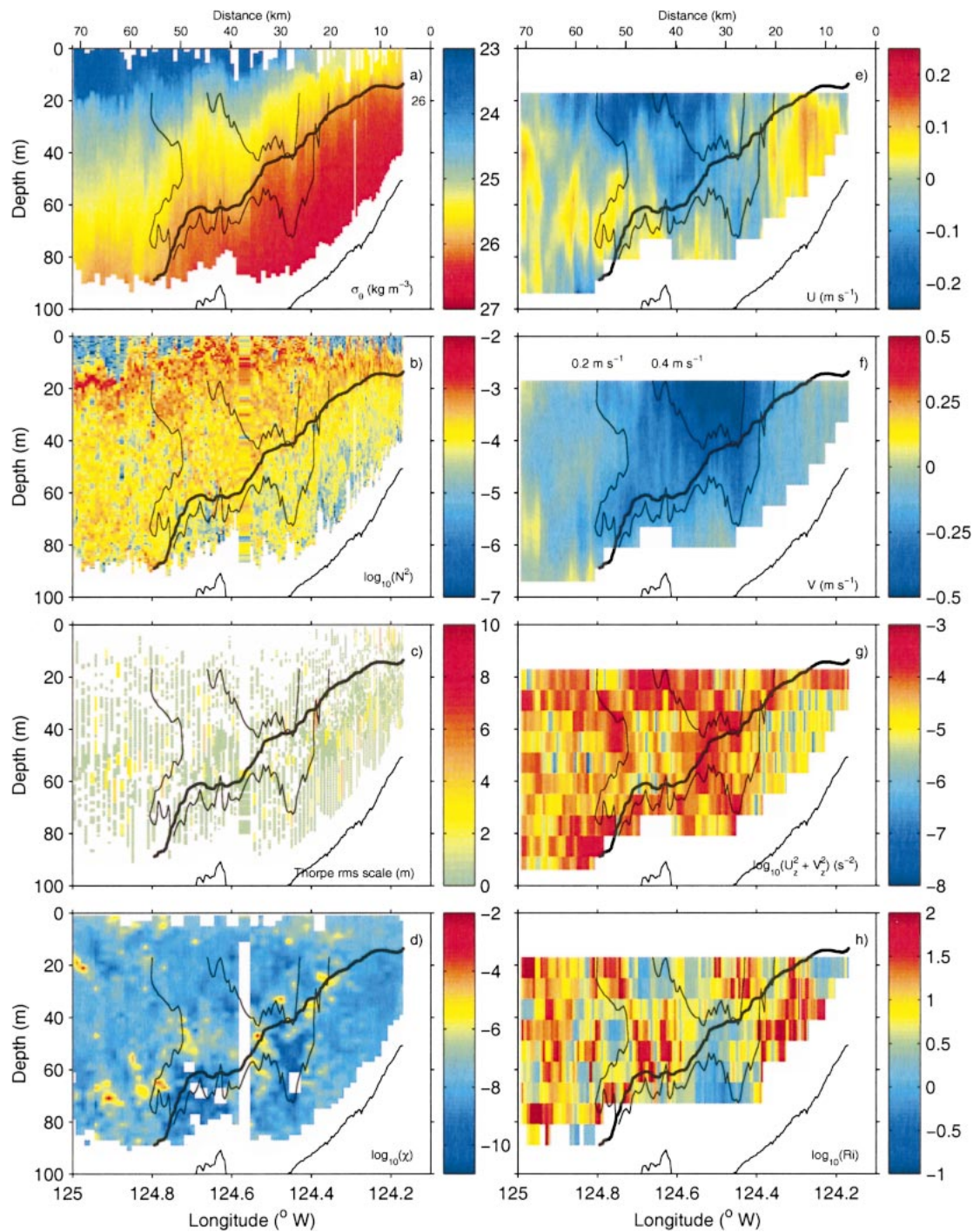


FIG. 7. As in Fig. 5, but for transect bb2line6.

is not as weak as in sbs1lineE, and Richardson numbers below 0.1 or Thorpe scales exceeding 8 m are not seen. Nevertheless, the scatterplots for bb2line6 (not shown) are qualitatively similar to Fig. 6. That is, elevated Thorpe scales are generally associated with weak stratification, large shear, and low Richardson number.

*b. Comparison to 24-Hz Sea-Bird data*

There is typically much less Thorpe-scale signal in the 24-Hz Sea-Bird data compared to MicroSoar, particularly at small and large Thorpe scales. This is a result of the slower response time of the Sea-Bird temperature

and conductivity sensors and to potential mixing that occurs in the duct leading to the conductivity sensor. These factors should result in the loss of displacement signal most notably for overturns that are small in vertical extent and for overturns in weakly stratified water, respectively. The latter are generally large, as seen just inshore and above Heceta Bank on line sbs1lineE (Fig. 5c), for example, in a region where stratification was weak (Fig. 5b) and Richardson numbers low (Fig. 5h). The corresponding overturns calculated from the Sea-Bird data (not shown) are both smaller and fewer in number.

Histograms of the number of overturns at each rms value (Fig. 8a) show this clearly: 1) the range of Thorpe scales calculated from MicroSoar data extends to smaller scales than those from the Sea-Bird data, and 2) overturns exceeding 4 m in extent are not seen in the Sea-Bird data. Therefore, not only does MicroSoar correct some of the undersampling of small Thorpe scales noted by Ullman et al. (2003), but it appears to better calculate Thorpe scales in regions of low stratification.

### c. Comparison to Chameleon data

Unfortunately, comparisons between Thorpe scales measured with the undulating platform and those from Chameleon are not very conclusive. Histograms (Fig. 8a) and probability density functions (PDFs) (Fig. 8b) of root-mean-square Thorpe scales indicate that Thorpe scales calculated on the Chameleon transects are smaller in size. However, PDFs of stability, as measured by the Richardson number, suggest that this disparity is due to a difference in energy levels between the transects (Fig. 8c).

This is not unreasonable, considering Moum et al. (1995) found order-of-magnitude differences in 1-day means of the estimated dissipation rate measured by shear probes on two vertical profilers over the same 3-day period on separate vessels operating within close proximity in the open ocean. They concluded that “natural variability can cause large differences in averages of  $\epsilon$  made over coincident  $O(100)$  profiles spaced reasonably evenly over the sampling period and located within several km of each other” (Moum et al. 1995). A more determined effort to collocate MicroSoar and loosely tethered free-falling microstructure instruments is needed to quantitatively compare these two instruments.

## 5. Summary

MicroSoar is a high-frequency instrument that, when mounted on SeaSoar, is able to make finescale thermal dissipation-rate measurements. In this paper, it has been shown that its high-resolution temperature and conductivity data significantly increase the ability to measure Thorpe scales, particularly scales of small vertical extent and those in regions of low stratification, compared to

those measured with the Sea-Bird 911+ CTD. Owing to the separation of the T and C probes, however, the density cannot be calculated directly, necessitating the development of a method employing lookup tables based on averaged Sea-Bird conductivity and density data.

Based on the two SeaSoar sections presented, it appears that the large Thorpe scales measured are associated with shear at the edge of the coastal jets and not with topographic features. The SeaSoar does not approach within 10 m of the bottom at best, however, so eddies smaller than 10 m in extent (i.e., smaller than the largest seen in the midwater column) associated with topography might not be seen with this undulating platform. It is likely that the available potential energy these bottom eddies represent is smaller, as stratification is typically much larger in the midwater column.

Unfortunately, due to the differences in turbulent energy between the Chameleon and SeaSoar transects, as evidenced by the differences in stability, it was not possible to relate Thorpe-scale results from the towed, undulating body to those from the more traditional free-falling profiler. Thorpe-scale analysis from instruments undulating at large horizontal speeds is not expected to be as accurate as those from free-falling instruments, the inability to measure smaller Thorpe scales (Fig. 8a) being an obvious shortcoming. The intent of the present analysis, however, is not to compete with measurements made from traditional instruments. Rather, we see the SeaSoar as a tool to quickly survey a much larger area for large overturns, identifying regions that can be examined repeatedly and in more detail using loosely tethered turbulence profilers or autonomous underwater vehicles.

We are presently using the Garrett–Munk internal wave spectrum, with parameters relevant to the Oregon shelf region, to examine the distribution of internal wave slopes. This will allow us to determine more clearly the effect of nonvertical attack angles on the measurement of potential overturns and will hopefully allow us to relax the  $1.0 \text{ m s}^{-1}$  vertical speed criterion. Future work will also include examining the energy made available to mixing by these eddies. In addition, by considering a more complete temporal history involving additional transects, including data from regions of simpler topography and with different wind regimes, the relationship between the onset of turbulence, represented by overturns, and its eventual manifestation as dissipation, may be examined.

*Acknowledgments.* We thank M. Willis, L. Fayler, D. Swensen, and T. Martin, OSU marine technicians, who were responsible for the operation of SeaSoar. Postprocessing the Sea-Bird data was done by R. O’Malley, and S. Pierce was responsible for the acoustic Doppler current profiler data. We appreciate the dedication of the officers and crew of R/V *Wecoma* in enabling us to tow SeaSoar through a region with substantial fishing

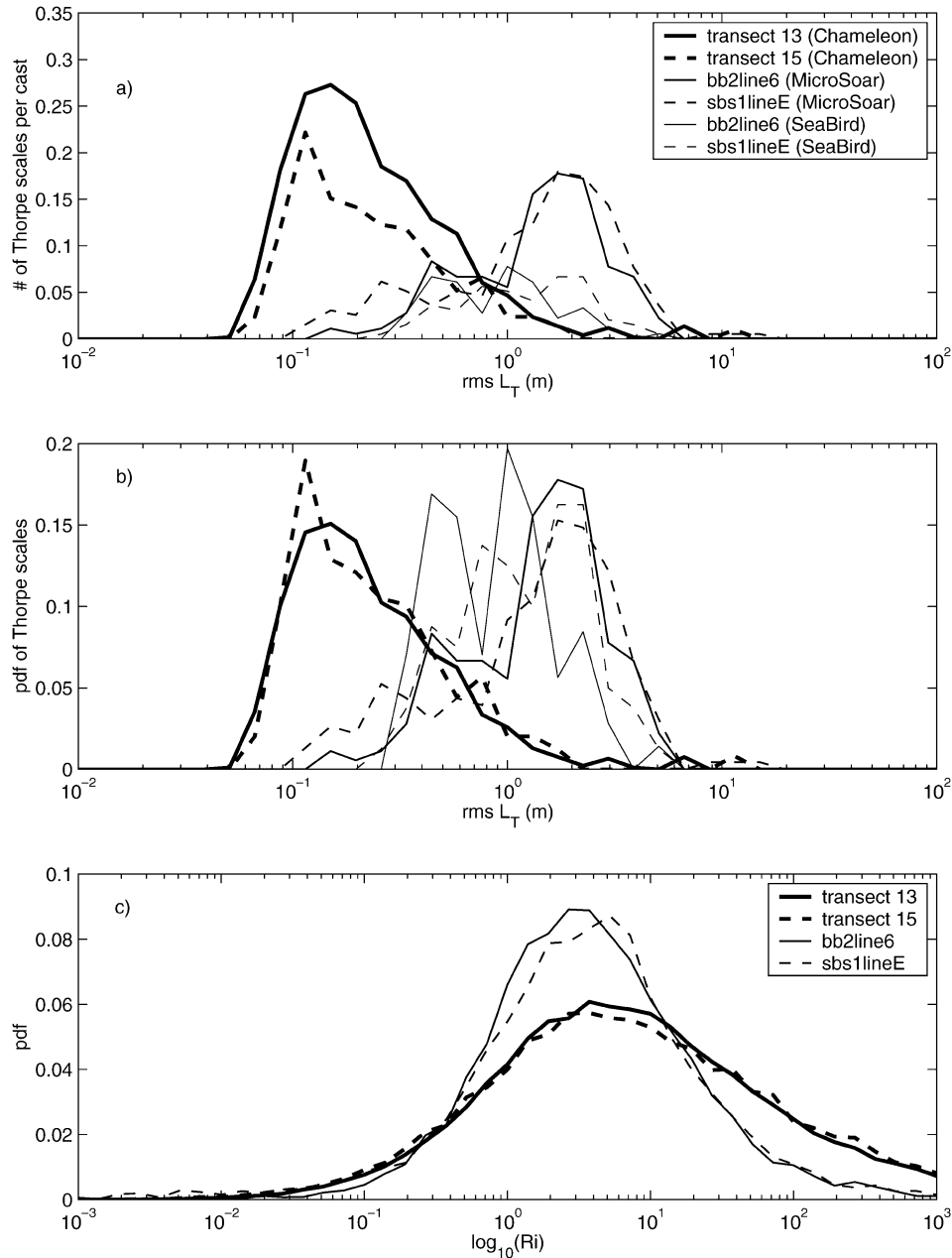


FIG. 8. Comparison of rms Thorpe scales and Richardson numbers for Chameleon and SeaSoar transects: (a) number of calculated Thorpe scales normalized by the number of drops, (b) probability density function of rms Thorpe scale, and (c) probability density function of Richardson number.

activity. We acknowledge Tom Dillon’s pioneering efforts in developing MicroSoar, and J. Moum and A. Perlin for helpful discussions and for providing Chameleon data with which to compare MicroSoar results. Finally, we thank the two anonymous reviewers for their thoughtful comments. This work is part of the Coastal Ocean Advances in Shelf Transport (COAST) project, funded by NSF as part of the Coastal Ocean Processes (CoOP) program through Grant OCE-9907854.

REFERENCES

Barth, J. A., S. D. Pierce, and R. L. Smith, 2000: A separating coastal upwelling jet at Cape Blanco, Oregon, and its connection to the California Current System. *Deep Sea Res.*, **47B**, 783–810.  
 ———, and the COAST Group, 2002: Investigation of the wind-driven coastal ocean off Oregon: A COAST overview. *Eos, Trans. Amer. Geophys. Union*, **83** (Fall Meeting Suppl.), Abstract OS61D-01, F701.  
 Caldwell, D. R., T. M. Dillon, and J. N. Moum, 1985: The rapid-

- sampling vertical profiler: An evaluation. *J. Atmos. Oceanic Technol.*, **2**, 615–625.
- Crawford, W. R., 1986: A comparison of length scales and decay times of turbulence in stable stratified flows. *J. Phys. Oceanogr.*, **16**, 1847–1854.
- Dillon, T. M., 1982: Vertical overturns: A comparison of Thorpe and Ozmidov length scales. *J. Geophys. Res.*, **87**, 9601–9613.
- , 1984: The energetics of overturning structures: Implications for the theory of fossil turbulence. *J. Phys. Oceanogr.*, **14**, 541–549.
- , J. A. Barth, A. Y. Erofeev, G. H. May, and H. W. Wijesekera, 2003: MicroSoar: A new instrument for measuring microscale turbulence from rapidly moving submerged platforms. *J. Atmos. Oceanic Technol.*, **20**, 1671–1684.
- Galbraith, P. S., and D. E. Kelley, 1996: Identifying overturns in CTD profiles. *J. Atmos. Oceanic Technol.*, **13**, 688–702.
- Gargett, A. E., 1994: Observing turbulence with a modified acoustic Doppler current profiler. *J. Atmos. Oceanic Technol.*, **11**, 1592–1610.
- Gregg, M. C., 1998: Estimation and geography of diapycnal mixing in the stratified ocean. *Physical Processes in Lakes and Oceans*, J. Imberger, Ed., Coastal and Estuarine Studies, Vol. 54. Amer. Geophys. Union, 305–338.
- , and W. C. Hess, 1985: Dynamic response calibration of Sea-Bird temperature and conductivity probes. *J. Atmos. Oceanic Technol.*, **2**, 304–313.
- Lueck, R., 1990: Thermal inertia of conductivity cells. *J. Atmos. Oceanic Technol.*, **7**, 741–755.
- May, G. H., 1997: MicroSoar: A high-speed microstructure profiling instrument. M.S. thesis, College of Oceanic and Atmospheric Sciences, Oregon State University, 227 pp.
- Moum, J. N., M. C. Gregg, R. C. Lien, and M. E. Carr, 1995: Comparison of turbulent kinetic energy dissipation rate estimates from two ocean microstructure profilers. *J. Atmos. Oceanic Technol.*, **12**, 346–366.
- , D. M. Farmer, W. D. Smyth, L. Armi, and S. Vagle, 2003: Structure and generation of turbulence at interfaces strained by internal solitary waves propagating shoreward over the continental shelf. *J. Phys. Oceanogr.*, **33**, 2093–2112.
- Newberger, P. A., D. R. Caldwell, T. M. Dillon, J. L. Cantey, S. D. Wilcox, M. D. Brown, and H. H. Dannelongue, 1984: The rapid-sampling vertical profiler. Tech. Rep. 84-5, College of Oceanography, Oregon State University, 409 pp.
- Paka, V. T., V. N. Nabatov, I. D. Lozovatsky, and T. M. Dillon, 1999: Oceanic microstructure measurements by “Baklan” and “Grif.” *J. Atmos. Oceanic Technol.*, **16**, 1519–1532.
- Pedlosky, J., 1979: *Geophysical Fluid Dynamics*. Springer-Verlag, 624 pp.
- Pierce, S. D., and J. A. Barth, 2002: Acoustic Doppler current profiler observations during the Coastal Ocean Advances in Shelf Transport (COAST) Survey I: R/V *Wecoma* cruise W0105C, 23 May to 13 June 2001. COAS Data Rep. 189, Ref. 2002-5, College of Oceanic and Atmospheric Sciences, Oregon State University, 129 pp.
- Pollard, R., 1986: Frontal surveys with a towed profiling conductivity/temperature/depth measurement package (SeaSoar). *Nature*, **323**, 433–435.
- Thorpe, S. A., 1977: Turbulence and mixing in a Scottish loch. *Philos. Trans. Roy. Soc. London*, **286A**, 125–181.
- , 1978: On the shape and breaking of finite amplitude internal gravity waves in a shear flow. *J. Fluid Mech.*, **85**, 7–31.
- Ullman, D. S., A. C. Dale, D. Hebert, and J. A. Barth, 2003: The front on the northern flank of Georges Bank in spring: 2. Cross-frontal fluxes and mixing. *J. Geophys. Res.*, **108**, 8010, doi:10.1029/2002JC001328.